How Changes in Cell Mechanical Properties Induce Cancerous Behavior

Parag Katira,[1] Muhammad H. Zaman,[2] and Roger T. Bonnecaze[1,*]

[1]*Department of Chemical Engineering, The University of Texas at Austin, Austin, Texas 78712, USA*
[2]*Department of Biomedical Engineering, Boston University, Boston, Massachusetts 02215, USA*

(Received 21 July 2011; published 11 January 2012)

Tumor growth and metastasis are ultimately mechanical processes involving cell migration and uncontrolled division. Using a 3D discrete model of cells, we show that increased compliance as observed for cancer cells causes them to grow at a much faster rate compared to surrounding healthy cells. We also show how changes in intercellular binding influence tumor malignancy and metastatic potential. These findings suggest that changes in the mechanical properties of cancer cells is the proximate cause of uncontrolled division and migration and various biochemical factors drive cancer progression via this mechanism.

DOI: 10.1103/PhysRevLett.108.028103 PACS numbers: 87.19.xj, 87.17.Aa, 87.18.Fx

The cancerous behavior of cells has been attributed to numerous biological factors that result in the malfunctioning of regulatory signaling pathways. The heterogeneity in these factors across different cancer types as well as different phenotypes of the same cancer makes it extremely difficult to chart a common mechanistic pathway for the induction and progression of cancerous behavior in cells [1,2]. Advances in biophysical techniques [3,4] have made it possible to observe the effect of specific biological factors on individual cell mechanical properties as well as the differences in the mechanical properties of healthy and cancerous cells [5–7]. It has been suggested that these changes play an important role in driving the uncontrolled growth and proliferation exhibited by cancer cells [8,9]. Understanding how and to what extent these mechanical changes induce and influence cancerous behavior would provide an improved physical description of cancer progression and help isolate the role of specific biological factors based on their influence on cell mechanical properties.

To this end, we have developed a computational model describing the life of a cell within a 3D tissue and applied it to observe the effect of changes in cell mechanical properties on cell fate decisions and the advent of cancerous behavior. Discrete cell models are extremely useful in tracking and predicting the behavior of individual cells as a function of their specific properties and have been successfully used to observe the shape and size evolution of tumors with single or multiple cancer cell phenotypes [10–12]. The discrete computational model we use here incorporates the following key features: (i) The described model tissue system is three-dimensional; (ii) the tumor cells are constantly interacting and competing for space with surrounding healthy cells; and (iii) cell growth is driven by cell mechanical properties, and cell fate decisions are stochastic functions of cellular stretch (as observed experimentally [13,14]) rather than an intrinsic cell growth rate culminating in cell division beyond a fixed size. These features make the model uniquely applicable for studying the effect of changes in mechanical properties of mutated cells in healthy tissue on tumor growth and metastasis in native environments.

Individual cells are modeled as viscoelastic shells around a liquid core representing a dense actin cortex surrounding a fluid cell interior [15]. Cells in contact adhere via intercellular bonds forming a flat interface [16]. The three-dimensional tissue is defined by a random distribution of points representing individual cells. The Voronoi polyhedra formed about these points provide the shape and size of corresponding cells. This formulation is shown schematically in Fig. 1. Each cell, when free in

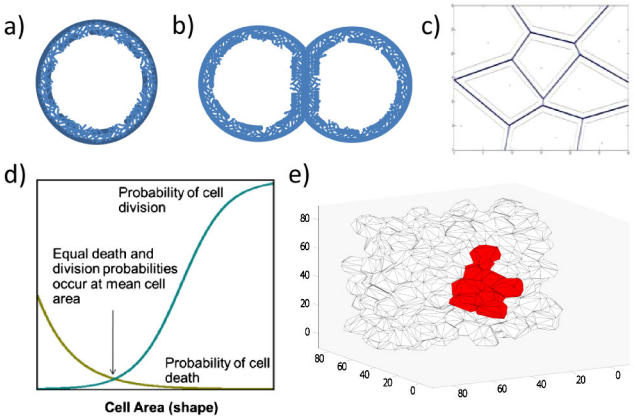

FIG. 1 (color online). (a) Schematic of a free cell in solution showing the viscoelastic actin cortex and the liquid core. (b) Schematic of two interacting cells and formation of an interface. (c) Schematic of multiple cells interacting and formation of Voronoi polyhedra defining the shape of cell—two-dimensional representations. (d) Plot showing the dependence of cell death and division probabilities on cell area qualitatively similar to observations by Chen *et al.* [13]. (e) Sectional view of the three-dimensional tissue model generated by discrete cell descriptions with a small bunch of tumor cells (red) near the center of the tissue. The axis scales are in microns.

solution, is a sphere of volume V_0. The average starting density of cells in a tissue is $1/V_0$. The cell shape and size change from spherical in free solution to polyhedral inside the tissue, and the resulting change in each cell's mechanical energy is given by

$$U_i = \frac{1}{2}k\frac{(A_i - A_{\rm sp})^2}{A_{\rm sp}} - \frac{1}{2}\sum_n A_j\sigma_j\gamma_j - C_1\ln\left(\frac{V_i}{V_0}\right). \quad (1)$$

The first term corresponds to the elastic energy of the stretched actin shell, k is the stiffness constant approximated by the product of the actin cortex elastic modulus E and its thickness y, A_i is the area of the cell, and $A_{\rm sp}$ is the area of the cell had it been spherical. The second term corresponds to the energy released by formation of intercellular bonds, n is the number of neighbors, and A_j, σ_j, and γ_j are the area of the interface, the bond density, and the bond energy between the cell and its jth neighbor, respectively. The third term corresponds to the work done by the osmotic pressure inside the cell as the cell volume changes from V_0 in free solution to V_i inside the tissue. Assuming an ideal gas relationship between the osmotic pressure of a dilute solution, $C_1 = \pi_0 V_0$, where π_0 is the osmotic pressure inside the cell when free in solution. The bending energy stored in the viscoelastic actin shell is assumed negligible since the actin cortex can rapidly reorganize to eliminate the bending stresses [17].

The cells rearrange to minimize the total energy $U = \sum U_i$. A Metropolis Monte Carlo thermalization algorithm [18,19] is used to obtain this minimum energy configuration of cells, with details given in Supplemental Materials [20]. Once the tissue is in this initial state, cells can either die, stay as they are, or divide into two daughter cells based on the following rules: (i) Cells with area equal to the average area of cells in the initial state, A_m, have equal probability p_0 of death or division, which is a measure of the average turnover period of cells within the tissue [20]; (ii) the probability of cell death increases as the area of a cell decreases; and (iii) the probability of cell division increases with the increase in cell area. The cell death and division probability functions are based on the experimental observations of Chen *et al.* [13] and are given, respectively, by

$$p_{\rm death} = p_0^{(A_i - A_{\rm sp}/A_m - A_{\rm sp})}, \quad (2)$$

$$p_{\rm div} = \left(1 + \frac{(1-p_0)}{p_0}\left[\frac{(1-p_0)}{(100-p_0)}\right]^{(A_i - A_m)/(A_m - A_{\rm sp})}\right)^{-1}. \quad (3)$$

Three possible mechanisms have been suggested for this dependence of cell death and division rates on cell area or stretch: (i) change in the number of surface bound signaling molecules which influence regulatory pathways [21,22], (ii) activation of signaling molecules and ion channels due to stretching of the cell membrane [23], and (iii) transmission of cellular stretch to the centrosome and the nucleus via microtubules and intermediate filaments [24]. Cell death within the tissue is represented by deleting the point corresponding to that cell, while cell division is represented by replacing the cell point by two points equally displaced from the original point along an arbitrary line. After a cycle of cell fate decisions for all the cells, the new configuration is again optimized for minimum energy, followed by another cycle of cell death and division. The model thus describes the life of cells comprising homogenous tissue. By changing the mechanical properties of a small group of mutant cells in the center of this tissue, we can observe the changes in cell and tissue behavior.

For studying tumorigenesis within a healthy host tissue as a function of changes in mechanical properties of a few cells, the model tissue must maintain tissue homeostasis, characterized by a steady average cell density. Standard parameter values describing the cell mechanical properties are summarized in Table I. We consider a periodically replicated, cubic tissue section containing 512 cells. Considering a larger tissue section with more cells does not affect the observed cell behavior (data not shown). We start with homogenous tissue, where all cells have the same actin cortex elasticity and intercellular adhesivity. Figure S1 [20] shows that the tissue maintains homeostasis over multiple cell fate and optimization cycles. Next, the elastic modulus of a few mutant cells near the center of the tissue is reduced to half [6,8,30] the value ($E =$ 250 Pa) of the surrounding healthy cells ($E = 500$ Pa). As long as the fraction of mutant cells at any time is less than 20%, the model tissue maintains homeostasis.

When the number of starting mutant cells is four or five cells, we do not observe a difference in their behavior as compared to normal cells [Fig. 2(a)]. However, when the initial number of mutant cells is increased to eight, we see a clear increase in the multiplication rate of these cells

TABLE I. Standard cell parameter values.

Cell property	Symbol	Value
Cell volume when free in solution	V_0	1000 μm^3
Healthy cell actin cortex elastic modulus	E	500 Pa, Refs. [15,25]
Actin cortex thickness	Y	1 μm, Refs. [15,25]
Intercellular bond density between healthy cells	$\sum$	200 μm^{-2}, Ref. [26]
Bond energy of intercellular bonds	γ	$20k_BT$, Refs. [27,28]
Osmotic pressure inside the cell when free in solution	π_0	100 Pa, Ref. [29]

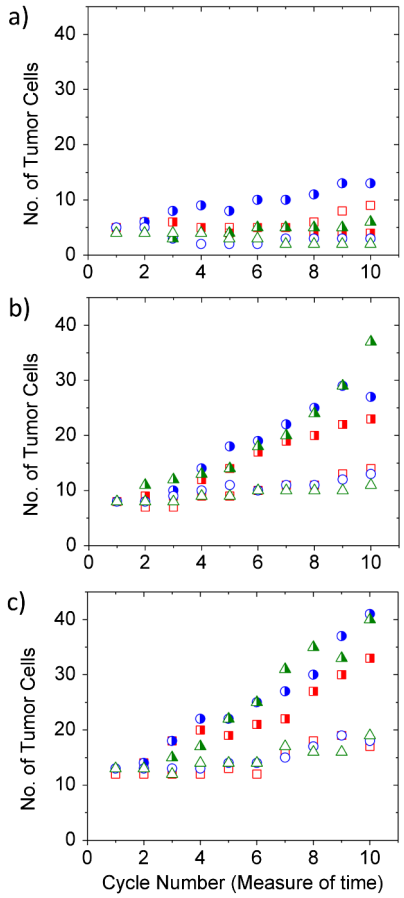

FIG. 2 (color online). Half-filled symbols represent the behavior of tumor cells, and hollow symbols represent the behavior of same cells had they been healthy. The different colors represent independent simulation runs with different starting configurations—(a) four (triangles) or five (circles and squares) starting tumor cells, (b) eight (triangles, circles, and squares) starting tumor cells, and (c) 12 (squares) or 13 (circles and triangles) starting tumor cells.

compared to healthy cells [Fig. 2(b)]. When the initial number is further increased to 12 or 13, we see an even greater multiplication rate [Fig. 2(c)]. Thus, lowering the cell elastic modulus, as seen experimentally for cancer cells [5,6,8,31], can drive these cells to multiply at an increased rate and compete for space within the tissue, just like actual tumors. Furthermore, there appears to be a threshold value for the starting number of mutant cells beyond which a tumor will most likely grow, as has been suggested previously [32]. The reason behind this observation is that, while surrounded by stiffer cells, compliant tumor cells cannot spread sufficiently, but, with an increase in neighboring compliant tumor cells, the resisting force against spread decreases and the tumor cells can attain larger surface areas. It should be noted that single or a few tumor cells less than the threshold value, though unstretched, can still divide at least at the same rate as healthy cells. The probability always exists that these cells might divide and, once their population crosses the threshold value, result in malignant tumors. We observed this phenomenon in one out of six simulations [data for three shown in Fig. 2(a)] with five or less initial tumor cells [circles data set in Fig. 2(a)].

Next, we consider the effect of intercellular bonding on tumor growth (Fig. 3). For 12 to 13 mutated cells with half the elastic modulus and an increased intercellular bond density between themselves ($\sigma = 300\ \mu\mathrm{m}^{-2}$) compared to surrounding healthy cells ($\sigma = 200\ \mu\mathrm{m}^{-2}$), we observe a slight increase in the tumor growth rate. On the other hand, a decrease in the intercellular bond density between mutant cells and other mutant as well as healthy cells ($\sigma = 100\ \mu\mathrm{m}^{-2}$) arrests tumor growth beyond a certain size. Also, the tumors where cells have a greater ability to bind to other mutant cells are relatively more compact and have low interfacial area to volume ratios (Fig. 4, top), while tumors where the cells have a decreased binding ability are more spread out and have higher interfacial area to volume ratios (Fig. 4, center). Interestingly, tumors, where the binding ability of the mutant cells is unchanged, are most spread out with high interfacial area to volume ratios and more isolated mutant cells apart from the main tumor mass (Fig. 4, bottom). This is because individual tumor cells that break off from the main tumor are more likely to survive within the healthy tissue with their binding ability maintained as compared to cells that have diminished binding ability. While there are no directly comparable experiments, these results can be qualitatively compared to a variety of observations, for, e.g., (i) tumors with increased

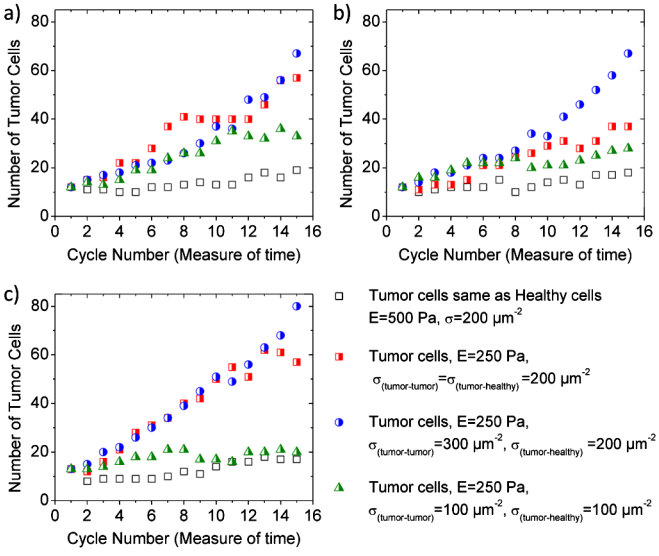

FIG. 3 (color online). These plots show the effect of changes in intercellular bonding on growth of tumors. Though stochastic in nature, the change in behavior of tumor cells is qualitatively similar for corresponding change in intercellular binding ability over multiple independent runs with different starting cell configurations as shown in (a) 12 initial tumor cells, (b) 12 initial tumor cells, and (c) 13 initial tumor cells.

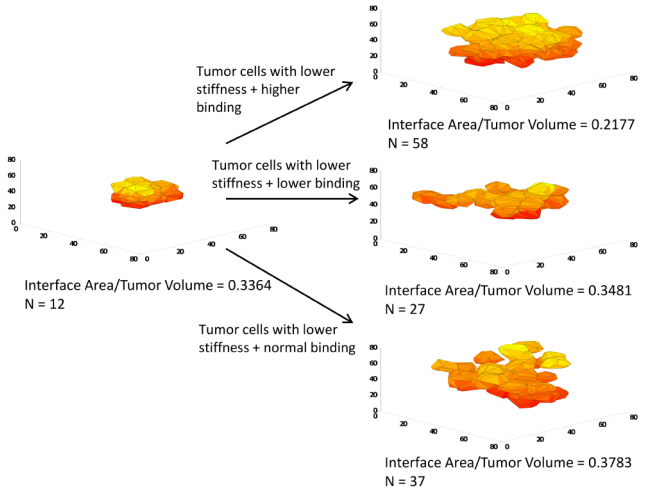

FIG. 4 (color online). The figure shows the shape and morphology of a tumor at the end of 14 cell cycles. The initial tumor morphology was the same for each of the three cases described (left panel). Right panel: Top—increased intercellular binding among tumor cells; middle—decreased intercellular binding among tumor cells as well as tumor and healthy cells; bottom—no change in tumor cell binding ability. The actin cortex elasticity of tumor cells is half the elasticity of healthy cell actin cortexes. It should be noted that the color gradient in cells along the z axis is only to generate some contrast between neighboring cells and is of no significance and that the white space in the plots is occupied by healthy tissue cells which are not plotted. The axis scales are in microns.

P-cadherin binding among mutant cells are more malignant [33,34] or (ii) formation of metastatic microtumors due to diminished mutant cell binding ability [8,32].

Previous models [35,36] of tumor growth describe cells as expanding viscoelastic spheroids that divide on reaching a target volume and cell death is largely neglected. Cell expansion rate is dependent on nutrient concentration and stresses due to crowding of cells as the tumor grows against a dissipative force in an unbounded environment. In the model described here, tumor cells grow within a homeostatic tissue where the average density of the cells is constant. Tumor cells compete for space with surrounding healthy cells, and mechanical property changes provide the forces required for the tumor cells to spread and multiply. Furthermore, cell death is an inherent part of our model key to maintaining tissue homeostasis. This model can be used to observe the effect of experimentally observed mechanical property changes between healthy and cancerous cells. Also, by identifying the influence of carcinogenic factors on a cell's mechanical properties, the specific role of these factors in tumor growth can be studied. Finally, this computational model can be used to observe general tissue dynamics as well. A homogenous tissue in homeostasis is modeled, and it is observed that the cell migrations within this tissue are random (Fig. S2 [20]). In contrast, modeling the dynamics of a nonhomogenous tissue section with a nutrient gradient shows that there is an increased division of cells near the nutrient-rich regions from where the cells migrate to the nutrient depleted regions and die (Fig. S2 [20]). The assumption here is that nutrients (primarily oxygen and glucose) keep the cells soft, while decreasing nutrient concentration increases the stiffness of the cells [37]. This phenomenon is clinically observed in multilayer epithelial tissues [38].

In summary, we show that an increase in the compliance of mutated cells, as observed for cancer cells [5,6], can cause them to grow at a much faster rate compared to surrounding healthy cells. We also show that changing intercellular binding influences the various stages of tumor growth and metastasis. These findings may bridge the gap between the numerous interdependent biochemical carcinogenic factors and the physical manifestation of tumor growth and proliferation by providing a mechanistic pathway for the cancerous behavior of cells.

The authors acknowledge the support from National Institutes of Health (R01CA132633-S109 and R01CA132633) to M. H. Z. and R. T. B.

*Corresponding author.
rtb@che.utexas.edu.

[1] J. E. Visvader, Nature (London) **469**, 314 (2011).
[2] C. Swanton, R. A. Burrell, and P. A. Futreal, Breast Cancer Res. Treat. **13**, 104 (2011).
[3] D. H. Kim, P. K. Wong, J. Park, A. Levchenko, and Y. Sun, Annu. Rev. Biomed. Eng. **11**, 203 (2009).
[4] M. R. K. Mofrad, Annu. Rev. Fluid Mech. **41**, 433 (2009).
[5] S. E. Cross, Y. S. Jin, J. Rao, and J. K. Gimzewski, Nature Nanotech. **2**, 780 (2007).
[6] E. L. Baker, J. Lu, D. H. Yu, R. T. Bonnecaze, and M. H. Zaman, Biophys. J. **99**, 2048 (2010).
[7] M. Lekka, P. Laidler, D. Gil, J. Lekki, Z. Stachura, and A. Z. Hrynkiewicz, Eur. Biophys. J. **28**, 312 (1999).
[8] A. Fritsch, M. Hockel, T. Kiessling, K. D. Nnetu, F. Wetzel, M. Zink, and J. A. Kas, Nature Phys. **6**, 730 (2010).
[9] T. Hampton, JAMA, J. Am. Med. Assoc. **299**, 276 (2008).
[10] H. Byrne, and D. Drasdo J. Math. Biol. **58**, 657 (2009).
[11] T. S. Deisboeck, Z. Wang, P. Macklin, and V. Cristini, Annu. Rev. Biomed. Eng. **13**, 127 (2011).
[12] C. L. Reis, J. M. Pacheco, M. K. Ennis, and D. Dingli, Integr. Biol. **2**, 41 (2010).
[13] C. S. Chen, M. Mrksich, S. Huang, G. M. Whitesides, and D. E. Ingber, Science **276**, 1425 (1997).
[14] L. E. Dike, C. S. Chen, M. Mrksich, J. Tien, G. M. Whitesides, and D. E. Ingber, In Vitro Cell. Dev. Biol. Animal **35**, 441 (1999).
[15] F. Wottawah, S. Schinkinger, B. Lincoln, R. Ananthakrishnan, M. Romeyke, J. Guck, and J. Kas, Phys. Rev. Lett. **94**, 098103 (2005).
[16] H. Honda, M. Tanemura, and T. Nagai, J. Theor. Biol. **226**, 439 (2004).
[17] S. Diez, G. Gerisch, K. Anderson, A. Muller-Taubenberger, and T. Bretschneider, Proc. Natl. Acad. Sci. U.S.A. **102**, 7601 (2005).

[18] N. Metropolis, A. W. Rosenbluth, M. N. Rosenbluth, A. H. Teller, and E. Teller, J. Chem. Phys. **21**, 1087 (1953).
[19] S. Kirkpatrick, C. D. Gelatt, and M. P. Vecchi, Science **220**, 671 (1983).
[20] See Supplemental Material at http://link.aps.org/supplemental/10.1103/PhysRevLett.108.028103 for a detailed description of the simulation algorithms and Figs. S1–S3.
[21] A. K. Fournier, L. E. Campbell, P. Castagnino, W. F. Liu, B. M. Chung, V. M. Weaver, C. S. Chen, and R. K. Assoian, J. Cell Sci. **121**, 226 (2008).
[22] A. Mammoto and D. E. Ingber, Curr. Opin. Cell Biol. **21**, 864 (2009).
[23] L. Formigli, E. Meacci, C. Sassoli, R. Squecco, D. Nosi, F. Chellini, F. Naro, F. Francini, and S. Zecchi-Orlandini, J. Cell. Physiol. **211**, 296 (2007).
[24] D. E. Ingber, J. Cell Sci. **116**, 1397 (2003).
[25] R. Ananthakrishnan, J. Guck, F. Wottawah, S. Schinkinger, B. Lincoln, M. Romeyke, T. Moon, and J. Kas, J. Theor. Biol. **242**, 502 (2006).
[26] Z. X. Li, D. L. Qiu, I. Sridharan, X. P. Qian, H. H. Zhang, C. B. Zhang, and R. Wang, J. Phys. Chem. B **114**, 2894 (2010).
[27] B. Zhu, S. Chappuis-Flament, E. Wong, I. E. Jensen, B. M. Gumbiner, and D. Leckband, Biophys. J. **84**, 4033 (2003).
[28] S. W. Byers, C. L. Sommers, B. Hoxter, A. M. Mercurio, and A. Tozeren, J. Cell Sci. **108**, 2053 (1995).
[29] G. T. Charras, M. Coughlin, T. J. Mitchison, and L. Mahadevan, Biophys. J. **94**, 1836 (2008).
[30] J. Guck *et al.*, Biophys. J. **88**, 3689 (2005).
[31] S. Suresh, Acta Mater. **55**, 3989 (2007).
[32] M. Basan, T. Risler, J. F. Joanny, X. Sastre-Garau, and J. Prost, HFSP J. **3**, 265 (2009).
[33] A. S. Ribeiro, A. Albergaria, B. Sousa, A. L. Correia, M. Bracke, R. Seruca, F. C. Schmitt, and J. Paredes, Oncogene **29**, 392 (2010).
[34] J. Paredes, A. Albergaria, J. T. Oliveira, C. Jeronimo, F. Milanezi, and F. C. Schmitt, Clin. Cancer Res. **11**, 5869 (2005).
[35] M. A. Stolarska, Y. Kim, and H. G. Othmer, Phil. Trans. R. Soc. A **367**, 3525 (2009).
[36] J. Galle, M. Loeffler, and D. Drasdo, Biophys. J. **88**, 62 (2005).
[37] S. S. An, C. M. Pennella, A. Gonnabathula, J. X. Chen, N. Wang, M. Gaestel, P. M. Hassoun, J. J. Fredberg, and U. S. Kayyali, Am. J. Physiol., Cell Physiol. **289**, C521 (2005).
[38] A. T. L. Lommel, *From Cells to Organs: A Histology Textbook and Atlas* (Kluwer Academic, Dordrecht, 2002).